ISSN (Online) 2456-1290

International Journal of Engineering Research in Mechanical and Civil Engineering (IJERMCE)

Volume 11 Issue 5 May 2024

On the Determination of Stress Triaxiality in a Cast Aluminum Alloy

[1] Azadeh J. Jazayeri, [2] Milan Zigo, [3] Eray Arslan

[1] [3] Vienna University of Technology, Institute for Mechanics and Mechatronics, Vienna, Austria
[2] Magna Steyr Fahrzeugtechnik GmbH & Co KG, Graz, Austria
Corresponding Author Email: [3] eray.arslan@tuwien.ac.at

Abstract*— This study presents a prediction of fracture behavior in the cast material AlSi10MnMg-T7 under multiaxial loading conditions. The main goal is to establish a triaxiality locus, which is a diagram illustrating the relationship between the equivalent plastic strain to fracture and the stress triaxiality factor. This factor is primarily defined as the ratio of the hydrostatic stress to the equivalent stress. The triaxiality locus provides in-depth insights into how the material's fracture behavior varies under different stress states. Experimental tests involving different specimen geometries are conducted to obtain essential data for the analysis and to facilitate the development of a Finite Element (FE) model. Quasi-static uniaxial tensile tests are performed on four specimen types, each featuring different forms of notches to induce different stress states in the specimens. The deformation up to fracture is captured using two high-speed digital cameras, and the displacement and strain data are calculated using a digital image correlation (DIC) system. Subsequently, the simulation results from the FE models are compared with the experimental measurements to validate the accuracy of the models. These FE models are then used to calculate the equivalent fracture strain and stress triaxiality factor with the help of collected test data. The calculations facilitate the generation of a stress triaxiality locus via a curve-fitting process. An exponential curve-fitting function is selected to appropriately relate the equivalent plastic strain to the fracture and stress state for the material. The results are also compared with those outlined in the FKM-Guideline, which is employed for the analytical calculation of mechanical component strength across different materials, and excellent agreement is obtained. By establishing the triaxiality locus and using experimental and numerical techniques, this study provides valuable data and insights for accurately predicting fracture strain and evaluating the stress state of structures made from the cast aluminum AlSi10MnMg-T7.

***Keywords* — Multiaxial loading, triaxiality locus, fracture behavior prediction, Finite Element simulation, AlSi10MnMg-T7, necking**

I. INTRODUCTION

Given the widespread use of cast aluminum materials in automotive industry and their exposure to complex multiaxial loading conditions, which increase the risk of ductile fracture [1], precise fracture detection and load estimation within intricate structures are essential concerns. Investigating material response, especially post-necking plastic deformation, is significant in the industrial context. This deformation, particularly post-necking, can significantly influence component designs' structural integrity and long-term reliability [2]. Crash management systems and low cycle fatigue analyses, in particular, significantly depend on plastic deformation, highlighting the critical importance of understanding material behavior during and after necking. With insights into material behavior, engineers can effectively identify and address potential failure scenarios, thereby enhancing the safety and durability of the end product. Although determining uniaxial fracture strain through standard tensile tests using simple specimens is relatively straightforward, predicting multiaxial fracture behavior based on these tests presents significant challenges. Furthermore, the fracture strain obtained from such standard specimens may not accurately and reliably reflect behavior under multiaxial loading conditions. Therefore, it may be useful to establish a stress triaxiality locus [3] that provides comprehensive information about the fracture stress concerning the multiaxial stress state of the material.

The triaxiality locus, a graphical representation that relates fracture equivalent plastic stress to the stress triaxiality factor, is a valuable tool for understanding the fracture behavior of materials under various loading conditions [4]. Establishing the triaxiality locus for a given material enables obtaining detailed information about its fracture behavior under different stress conditions, thereby facilitating more accurate predictions. The stress triaxiality factor (η), expressed as the ratio of hydrostatic stress to equivalent stress (von Mises in our case), significantly impacts fracture strain, as evidenced by prior research [5] and calculated by the following equation [6]:

$$\eta = \frac{(\sigma_1 + \sigma_2 + \sigma_3)/3}{\sqrt{[(\sigma_1 - \sigma_2)^2 + (\sigma_2 - \sigma_3)^2 + (\sigma_3 - \sigma_1)^2]/2}} \quad (1)$$

where σ_i is principal stress.

Given the wide range of alloyed materials utilized in industrial contexts, creating a detailed table outlining their individual characteristics is not feasible. As a result, the standard approach involves conducting experiments and analyses specific to each material, mainly focusing on understanding its fracture behavior. On the other hand, some guidelines, such as the FKM [7,8], propose analytical methods to establish the triaxiality locus for some structural steel and aluminum. The FKM guideline, short for the German name "Forschungskuratorium Maschinenbau"

ISSN (Online) 2456-1290

International Journal of Engineering Research in Mechanical and Civil Engineering (IJERMCE)

Volume 11 Issue 5 May 2024

(Research Association of Mechanical Engineering) [7], serves as a calculation tool with a systematic approach and is frequently used in industrial applications. This guideline presents an empirical equation providing an exponential triaxiality locus for the material AlSi1MgMn and its extensive database for the required material properties [9,10]. However, the guideline does not provide any comparison to experimental results [11]. Therefore, the validation of this empirical approach and, in particular, the comparison of the triaxiality behavior obtained for AlSi10MnMg-T7, the casting material used in this study, with the results of the FKM guideline may be required. The objective of this study is to develop a reliable multiaxial fracture analysis for the material AlSi10MnMg-T7 and to compare the obtained results with the FKM guideline results (for AlSi1MgMn) for a validation.

This study aims to particularly understand the behavior of the tested material AlSi10MnMg-T7 from the necking initiation until a fracture occurs, offering a comprehensive insight into its reactions under various stress conditions. These insights hold significant value for multiple purposes, including predicting fractures, analysing failures, and validating models. Hence, this study focuses on conducting a stress triaxiality analysis of AlSi10MnMg-T7 to evaluate the stress state of structures subjected to complex loading conditions and to facilitate the prediction of fracture strain under multiaxial stress states in the tensile region, neglecting the effect of the Lode angle parameter.

Obtaining a thorough triaxiality locus involves performing experiments across various stress conditions, which can cause significant costs [6]. Therefore, conducting at least four tests, including uniaxial tension, pure shear, combined shear-tension, and notched specimens, is recommended to analyse the experimental data and develop the locus curve [6] with a low experiment cost but high accuracy. This experimental approach was also employed in similar research studies [3,5,12-14] for different ductile materials. During the experiments using extensometers and a Digital Image Correlation (DIC) system, as opposed to conventional strain measurement techniques, ensure accurate measurement of deformations at critical points on the specimens. Based on the measurement outcomes, Finite Element (FE) models are constructed to identify data points for fracture strain and stress triaxiality factor, facilitating the development of a stress triaxiality locus for the material using curve fitting models [15].

Two curve-fitting approaches may be considered to generate the triaxiality locus by using the test results. The first approach involves dividing the data into three different regions, each of which can be described by different nonlinear functions [6,16], for curve fitting, as illustrated in Fig. 1 [14,17,18]. The second approach requires exponential curve fitting (see Fig. 2 as an example for Aluminum alloy) [19]. In the present study, an exponential fitting function is selected to establish the relationship between equivalent plastic strain to fracture and the stress state for the AlSi10MnMg-T7 alloy, as the results exhibit greater consistency with it. It is noted that only the tensile part of the locus is studied in this study, excluding the compression part. An extensive literature search [14,19,20] has also shown that cast materials generally exhibit locus distributions similar to those in Fig. 2.

II. UNIAXIAL TENSILE TEST

Quasi-static uniaxial tensile experiments are carried out using four different geometrical configurations, denoted as specimen types A, B, C, and D, all having a consistent thickness of 3.3 mm, as depicted in Fig. 3, for the material AlSi10MnMg-T7. Different specimen geometries are essential for assessing different fracture criteria, including pure shearing, uniaxial tension, and combined shearing and tension scenarios, as depicted in Fig. 1. To assure the reliability and consistency of the data, three trials are conducted under the same conditions for each type of specimen during the measurements.

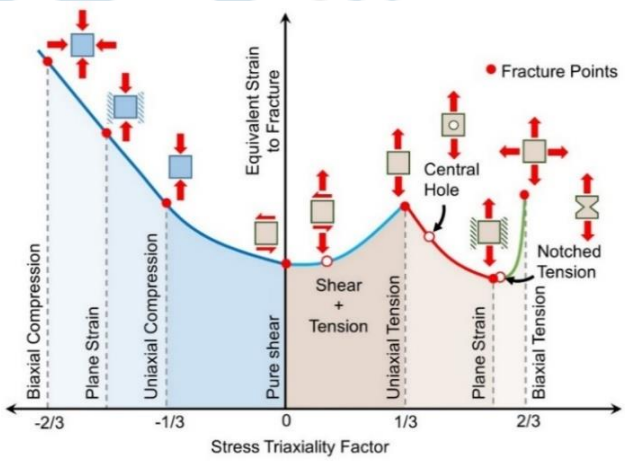

Fig. 1. An example of "stress triaxiality locus" [17,18]

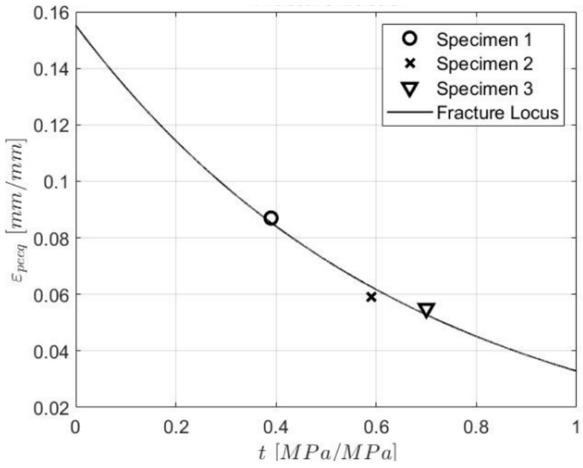

Fig. 2. Triaxiality locus of AlSi10 aluminum alloy [19]

ISSN (Online) 2456-1290

International Journal of Engineering Research in Mechanical and Civil Engineering (IJERMCE)

Volume 11 Issue 5 May 2024

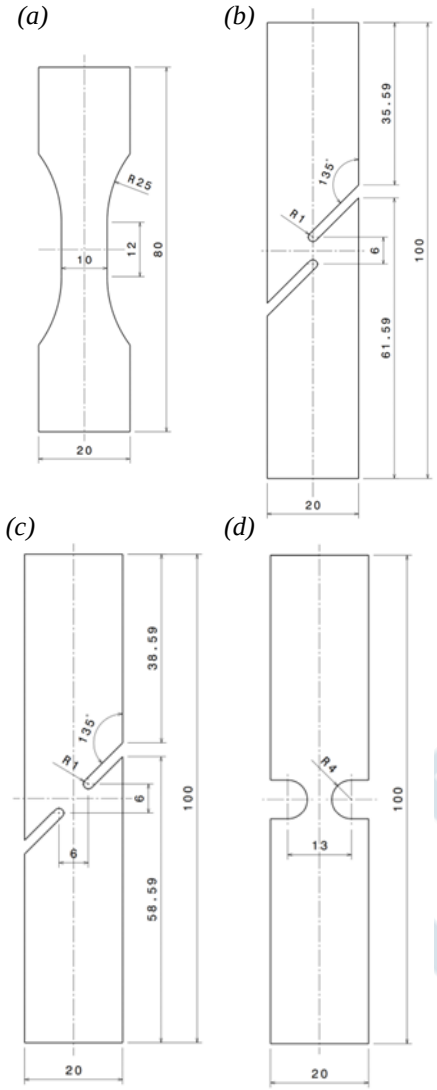

Fig. 3. Specimen type (a) A (uniaxial tensile), (b) B (pure shear), (c) C (45° shear-tensile), and (d) D (notched)

During the tests with increasing applied axial force, deformation is recorded using an extensometer with a 10mm gauge length. Moreover, high-resolution cameras equipped with a Digital Image Correlation (DIC) system were employed to capture the experiment at high speeds, facilitating post-processing analysis to measure displacement, area reduction, and true strain in specific regions and points of interest due to emerging fracture. As an example, the distribution of the first principal strain on the specimen surface in the DIC post-process for specimen B is presented in Fig. 4. In the post-processing stage, the response variables can be measured locally for the desired point, and therefore, the exact location of the fracture can be precisely determined. This point will be referred to as "the measurement point" in the following analyses. The comprehensive report generated from these experiments includes the engineering stress-engineering strain diagrams for all specimens. It provides insights into the distribution of various responses, such as principal strain components, elongation, and area reduction, within critical regions.

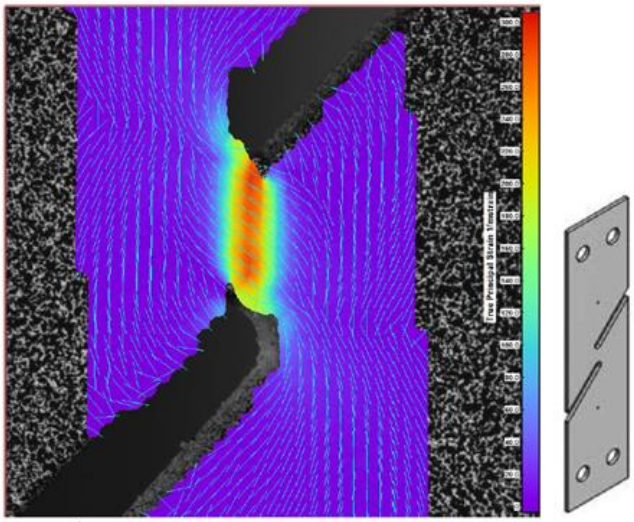

Fig. 4.1st principal strain distribution by DIC in specimen B

During the tests, uniaxial loading is progressively applied until the specimens have a complete fracture since the current analysis explicitly focuses on the fracture strain and its corresponding stress state. True stress and logarithmic strains are exclusively calculated for specimen type A, which corresponds to the standard tensile test specimen (see dashed line in Fig. 7). This graphical representation also leads to determining the material's modulus of elasticity and yield stress. The test results also significantly contribute to defining the stress-plastic strain relationship, clarifying the material's hardening behavior. The material data generalized from these test results for the plastic regions are employed in all FE simulations, encompassing specimens B-D. It is noted that while a true stress-strain curve can be constructed for specimen A with the measurements directly, computing stresses and strains for the deformed bodies of the other specimen types without FE models presents considerable challenges. Consequently, force-true principal strain relations for specimens B and C and force-maximum principal strain relations for specimens D are measured at measurement points with the help of the DIC system (see dashed lines in figures 8-10). These data will be used to validate the FE models and identify fracture points in the corresponding specimens.

Identifying the initial necking point, which is crucial in the process, is conventionally accomplished through the uniaxial tensile test, denoted as specimen A in this study. The theory governing the initiation of necking indicates that the tangent at the necking point intersects the horizontal axis precisely at a distance of one from the necking point [21]. This, along with the nominal stress-strain curve and data from the report, offers an understanding of the true strain value for the necking initiation point and the corresponding nominal stress.

ISSN (Online) 2456-1290

International Journal of Engineering Research in Mechanical and Civil Engineering (IJERMCE)

Volume 11 Issue 5 May 2024

III. FINITE ELEMENT SIMULATION

Finite Element (FE) models are developed to determine the "equivalent plastic strain to fracture" and its corresponding "stress triaxiality factor" for each type of specimen and establish the triaxiality locus for AlSi10MnMg-T7. Although initial values of these variables can be theoretically computed for different specimen types based on several assumptions [5], achieving more realistic results necessitates analysing FE analysis, considering the highly nonlinear deformation behavior of the material under multiaxial loading beyond the necking region. In this study, FE models of each type of specimen are prepared in ABAQUS/CAE to simulate them in corresponding loading conditions.

The models are structured to include symmetry planes, simplifying complexity and reducing computational costs, for all specimen types. Specifically, one-eighth of the original geometry is utilized for specimens A (see also Fig. 5) and D, considering symmetry conditions, while specimens B and C are modelled with half of their thickness.

To simulate a monotonically increasing displacement in the axial direction, reference points are defined, each associated with an area that assures the loading conditions observed in the experiments, as demonstrated for specimen A in Fig. 5 for an example. Material properties such as Modulus of Elasticity and hardening parameters for the cast material AlSi10MnMg-T7, derived from the test results of specimen A, are implemented into ABAQUS. The DIC analysis leads to the detection of the initial fracture point, the so-called measurement point (see Fig. 5). Then, the triaxiality factor and equivalent plastic strain to fracture are calculated at this measurement point in the FE analysis.

It is noted that the developed FE models do not include any damage model and, therefore, cannot determine the onset of specimen fracture. As a result, fracture initiation points are defined in experimental tests (specifically by the DIC analysis) and considered termination criteria for the simulations.

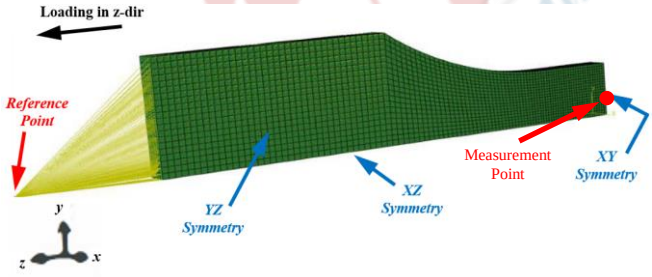

Fig. 5. FE model of specimen A in ABAQUS/CAE

Beginning with specimen A, the focus is directed towards the behavior of its cross-section at its center. For the further investigation of the stresses in this specimen, the corner nodes are denoted as A, B, C, and D, as depicted in Fig. 6. Point C aligns with the measurement position in the tensile test, while point B is positioned in the middle core of the model, where fracture initiation is expected [22,23]. As shown in Fig. 7, at the moment of final fracture, the core of the specimen (Node B) undergoes the highest stress, emphasizing the importance of attentively considering this phenomenon during the design phase. Disregarding the stress concentration at the mid-core could lead to underestimated safety margins and potentially result in premature failure. However, the primary objective of this research is to establish the stress triaxiality locus. Thus, node C, corresponding to the measurement point in the tensile test on the surface (refer to Fig. 6), is chosen to study for further analysis. This approach is consistently applied to all other specimens to ensure that the selected node corresponds to the measurement point in the experiment.

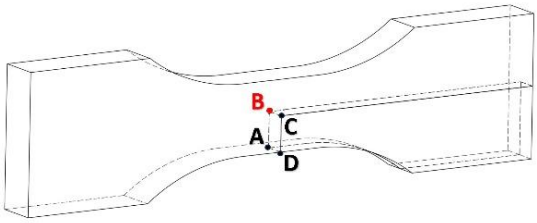

Fig. 6: One-eighth model of specimen A and the corresponding corner nodes

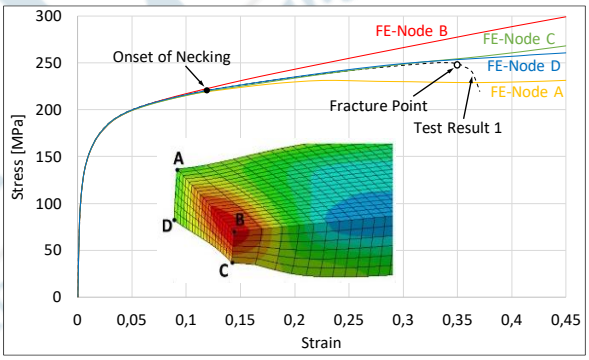

Fig. 7. Comparison of test result (dashed line) and FE simulation results (solid lines) for specimen A (true stress-strain curves)

The accuracy of the FE models is validated by comparing them with the corresponding test results. The true stress-true strain relationship for specimen A (Fig. 7) and the force-principal strain relationships for specimens B, C, and D are compared to the test results, as shown in Figs. 8-10. Following this validation, the models establish the correlation between equivalent plastic strain to fracture and the stress triaxiality factor.

IV. STRESS TRIAXIALITY LOCUS

The tensile part of the locus is studied in this study, excluding the compression part, since the experiment involves only tensile testing. In the FE analysis, the selection of appropriate nodes on the surface of each specimen, corresponding to the specimens' measurement points, is conducted. ABAQUS software [24] is utilized to extract

ISSN (Online) 2456-1290

International Journal of Engineering Research in Mechanical and Civil Engineering (IJERMCE)

Volume 11 Issue 5 May 2024

"equivalent plastic strain" (PEEQ) and "stress triaxiality" (TRIAX) values for these designated nodes, representing the test's measurement points, as shown in Fig. 11. The marked points correspond to relevant fracture points based on the test results.

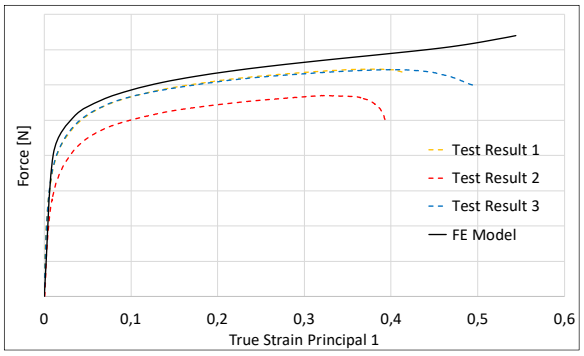

Fig. 8. Comparison of test results and FE simulation result for specimen B at the measurement point

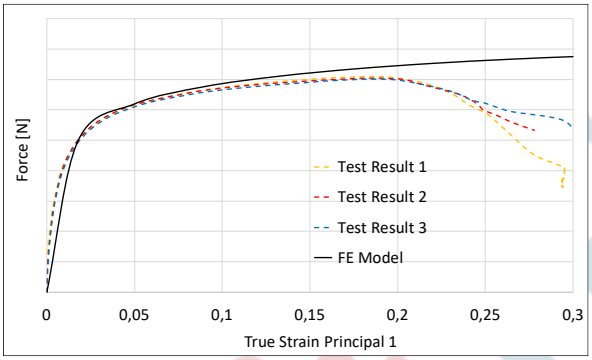

Fig. 9. Comparison of test results and FE simulation result for specimen C at the measurement point

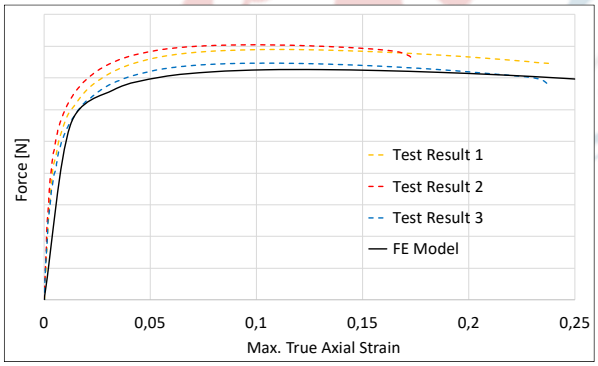

Fig. 10. Comparison of test results and FE simulation result for specimen D at the measurement point

It is noted that while the theoretical stress triaxiality values for each specimen can be calculated using Eq. (1), practical applications often witness variations in this value during loading, particularly post-necking, due to local dislocations at the cross-section. Interestingly, the observed stress triaxiality values from FE analysis, as depicted in Fig. 11, for specimen C are higher than the theoretical values, possibly due to unique properties inherent in the examined cast aluminum material. Similarly, in the case of notched specimen D, the stress triaxiality value is found to be less than the expected value, likely attributed to the radius of the notch. It's reasonable to anticipate that specimens with sharper notches would exhibit higher values.

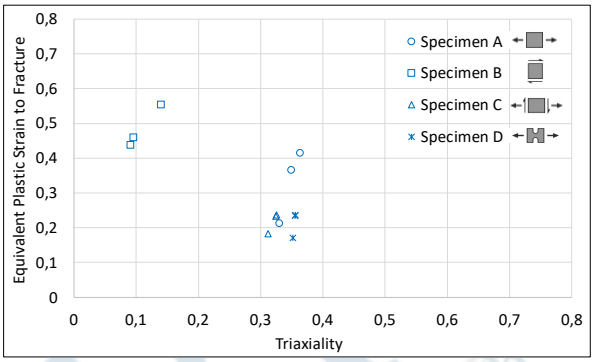

Fig. 11. Equivalent plastic strain vs stress triaxiality at fracture for specimens A-D (at measurement points on the surfaces)

The data points at equivalent plastic strain at fracture, and the corresponding triaxiality factors in Fig. 11 are used for the further curve-fitting process and to plot the triaxiality locus. The curve-fitting method utilized, derived from the reduced JC damage model [22,25,26], employs an exponential function:

$$\bar{\varepsilon}_f = D_1 + D_2 e^{D_3 \eta} \quad (2)$$

where D_1-D_3 are constants determined by minimizing the error between the exponential function and the data points in Fig. 11 for the curve fitting. The resulting curve, which is the triaxiality locus of the material AlSi10MnMg-T7, is presented in Fig. 12. In this figure, the current locus (blue solid line) is also compared with the corresponding locus that was also given in the FKM guideline for AlSi1MgMn (red solid line) [7]. An excellent agreement between the two results is obtained. The FKM guideline lacks direct comparison with experimental results, requiring users to trust the procedure without empirical validation [11]. Consequently, this study serves as a means of validating the guideline's applicability, specifically for the distinct material AlSi10MnMg-T7.

V. CONCLUSION

Four different specimen types produced from cast material AlSi10MnMg-T7, including the conventional rectangular cross-sectional uniaxial, pure shear, combined shear-tensile angled at 45°, and notched specimens, are subjected to uniaxial quasi-static tensile testing. The measurements serve as the basis for subsequent FE analysis. FE simulations use acquired test results to validate accuracy under similar loading conditions and determine critical load and strain leading to specimen fracture. Equivalent plastic strain and stress triaxiality factor are calculated for each specimen type

ISSN (Online) 2456-1290

International Journal of Engineering Research in Mechanical and Civil Engineering (IJERMCE)

Volume 11 Issue 5 May 2024

at their test measurement points to lead the basis for a comprehensive stress triaxiality locus for AlSi10MnMg-T7.

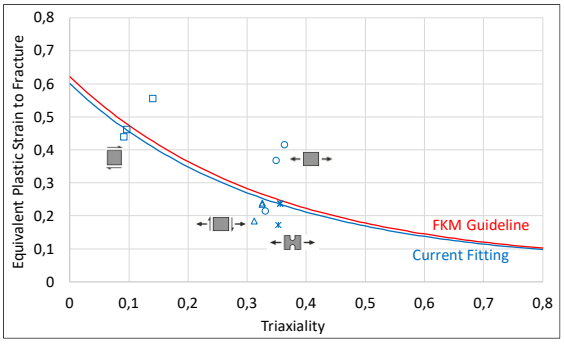

Fig. 12. Stress triaxiality locus of AlSi10MnMg-T7 compared to FKM fitting for AlSi1MgMn

Initial failure in specimen A occurs in the central core, yet the surface node is selected for stress triaxiality determination, aligning with surface measurement used in experimental trials. Various functions proposed in the literature are considered during the data fitting process, emphasizing selecting one that best aligns with the material's behavior. For AlSi10MnMg-T7, the exponential function for the triaxiality locus emerges as the most suitable choice. The simulation and fitting results for the locus are also compared with the FKM guideline, and excellent agreement is obtained. Consequently, this research verifies the applicability of the FKM guideline specifically for the AlSi10MnMg-T7 material. Further exploration into the Lode angle's implications on stress triaxiality analysis, alongside investigation into anisotropic behavior and strain rate effects, promises valuable insights and warrants comprehensive examination.

ACKNOWLEDGEMENTS

This study is financially supported by the research project titled “Plasticity and Fracture Analyses of a Cast Material (PafCast)” with project number 2259258, a collaboration between MAGNA STEYR Fahrzeugtechnik GmbH & Co KG (Graz) and TU Wien.

REFERENCES

[1] P. Foti, N. Razavi, A. Fatemi, and F. Berto, "Multiaxial fatigue of additively manufactured metallic components: A review of the failure mechanisms and fatigue life prediction methodologies," Progress in Materials Science, vol. 137, pp. 101126, 2023.

[2] S. Rafiee, "Experimental and theoretical prediction of a micromechanics-based stress state dependent failure model for ductile materials in ABAQUS, LS-DYNA and PAM-CRASH," in Simulation in vehicle, Baden, Germany, 2022.

[3] Y. Bao, and T. Wierzbicki, "On fracture locus in the equivalent strain and stress triaxiality space," International Journal of Mechanical Sciences, vol. 46, pp. 81-98, 2004.

[4] P. W. Bridgman, "Studies in large plastic flow and fracture: with special emphasis on the effects of hydrostatic pressure," Harvard University Press, 1964.

[5] Y. Peng, X. Chen, S. Peng, C. Chen, J. Li, and G. Liu, "Strain rate-dependent constitutive and low stress triaxiality fracture behavior investigation of 6005 Al alloy," Hindawi - Advances in Materials Science and Engineering, Nr. Article ID 2712937, 2018.

[6] M. Asadi, F. H. Aboutalebi, and M. Poursina, "A comparative study of six fracture loci for DIN1623 St12 steel to predict strip tearing in a tandem cold rolling mill," Archive of Applied Mechanics, vol. 91, pp. 1859-1878, 2021.

[7] FKM (Forschungskuratorium Maschinenbau), Analytical Strength Assessment of Components, VDMA Verlag, 6th revised edition, 2012.

[8] M. Wächter, C. Müller, and A. Esderts, Angewandter Festigkeitsnachweis nach FKM-Richtlinie, Springer Vieweg, 2021.

[9] M. Fiedler, M. Wächter, I. Varfolomeev, M. Vormwald, and A. Esderts, "Rechnerischer Bauteilfestigkeitsnachweis unter expliziter Erfassung nichtlinearen Werkstoff-Verformungsverhaltens," VDMA-Verlag, AiF-Projekt 17612, 2015.

[10] B. Hänel, E. Kullig, M. Vormwald, C. Versch, A. Esderts, K. Hinkelmann, D. Siegele, and J. Hohe, "Verbessertes Berechnungskonzept FKM-Richtlinie. Ein verbessertes Berechnungskonzept des statischen Festigkeitsnachweises und des Ermüdungsnachweises für die nichtgeschweißte und geschweißte Maschinenbauteile nach der FKM-Richtlinie Festigkeitsnachweis," Technical Report FKM-Vorhaben 282, FKM-Heft 306, VDMA-Verlag, 2010.

[11] S. Koechlin, "FKM Guideline: strengths, limitations and experimental validation," Procedia Engineering, vol. 133, pp. 309 – 319, 2015.

[12] M. Kõrgesaar, J. Romanoff, H. Remes, and P. Palokangas, "Experimental and numerical penetration response of laser-welded stiffened panels," International Journal of Impact Engineering, vol. 114, pp. 78-92, 2018.

[13] H. Mae, X. Teng, Y. Bai and T. Wierzbicki, "Ductile fracture locus of AC4CH-T6 cast aluminium alloy," Computational Materials Science and Surface Engineering, vol. 1, pp. 100-105, 2009.

[14] M. Kõrgesaar, "The effect of low stress triaxialities and deformation paths on ductile fracture simulations of large shell structures," Marine Structures, vol. 63, pp. 45-64, 2019.

[15] F. Andrade, S. Conde, M. Feucht, M. Helbig, and A. Haufe, "Estimation of stress triaxiality from optically

measured strain fields," in Proceedings of the 12th European LS-DYNA Conference, Koblenz, Germany, pp. 14-16, 2019.

[16] Z. A. Mehari, and J. Han, "Numerical prediction of ductile fracture during the partial heating roll forming process of DP980," International Journal of Fracture, vol. 234, pp. 97-112, 2022.

[17] E. Arslan. [Online]. Available: www.tuwien.at/en/mwbw/mec/e325-01-research-unit-of-technical-dynamics-and-vehicle-system-dynamics/research-projects/magna-triax.

[18] E. Arslan, and M. Haskul, "Fracture behavior prediction of a high-strength aluminum alloy under multiaxial loading," in the 9th World Congress on Mechanical, Chemical, and Material Engineering (MCM'23), London, 2023.

[19] L. Fraccaroli, M. N. Mastrone, and F. Concli, "Calibration of the fracture locus of an AlSi10 aluminum alloy," WIT Transactions on The Built Environment, vol. 196, pp. 3-10, 2020.

[20] J. Papasidero, V. Doquet, and D. Mohr, "Ductile fracture of aluminum 2024-T351 under proportional and non-proportional multi-axial loading: Bao–Wierzbicki results revisited," International Journal of Solids and Structures, vol. 69, pp. 459-474, 2015.

[21] A. Mendelson, Plasticity: Theory and Application, New York: Macmillan.

[22] H. Mae, X. Teng, Y. Bai, and T. Wierzbicki, "Comparison of ductile fracture properties of aluminum castings: Sand mold vs. metal mold," International Journal of Solids and Structures, vol. 45, pp. 1430-1444, 2007.

[23] J. M. Choung, and S. R. Cho. "Study on true stress correction from tensile tests." Journal of Mechanical Science and Technology, vol. 22, pp. 1039-1051, 2008

[24] Abaqus Documentation, 2022.

[25] Y. Abushawashi, X. Xiao, and V. Astakhov, "A novel approach for determining material constitutive parameters for a wide range of triaxiality under plane strain loading conditions," International Journal of Mechanical Sciences, vol. 74, pp. 133-142, 2013.

[26] J. R. Rice, and D. M. Tracey, "On the ductile enlargement of voids in triaxial stress fields," Journal of the Mechanics and Physics of Solids, vol. 17, pp. 201-217, 1969.